Experimental Study of Concurrent Data and Wireless Energy Transfer for Sensor Networks

M. Yousof Naderi,* Kaushik R. Chowdhury,* Stefano Basagni,*
Wendi Heinzelman,† Swades De,‡ and Soumya Jana§

*Department of Electrical and Computer Engineering, Northeastern University, Boston, MA, U.S.A
E-mail: {naderi, krc, basagni}@ece.neu.edu
†Department of Electrical and Computer Engineering, University of Rochester, Rochester, NY, U.S.A
E-mail: wheinzel@ece.rochester.edu
‡ Department of Electrical Engineering, IIT Delhi, New Delhi, India. E-mail: swadesd@ee.iitd.ernet.in
§Department of Electrical Engineering, IIT Hyderabad, Hyderabad, India. E-mail: jana@iith.ac.in

Abstract—**Wireless transfer of energy through directed radio frequency waves has the potential to realize perennially operating sensor nodes by replenishing the energy contained in the limited on-board battery. However, the high power energy transfer from energy transmitters (ETs) interferes with data communication, limiting the coexistence of these functions. This paper provides the first experimental study to quantify the rate of charging, packet loss due to interference, and suitable ranges for charging and data communication of the ETs. It also explores how the placement and relative distances of multiple ETs affect the charging process, demonstrating constructive and destructive energy aggregation at the sensor nodes. Finally, we investigate the impact of the separation in frequency between data and energy transmissions, as well as among multiple concurrent energy transmissions. Our results aim at providing insights on radio frequency-based energy harvesting wireless sensor networks for enhanced protocol design and network planning.**

I. INTRODUCTION

Wireless Sensor Networks (WSNs) are a fundamental building block of the Internet of Things (IoT) and a key enabler for cyber physical and pervasive computing systems. However, sensor nodes are typically battery-powered, and their limited energy affects protocol design, sacrificing throughput, bandwidth usage, and reliability to the need for extended network lifetime through judicious use of energy. Since it is often difficult, if not impossible, to access the sensor nodes and replace their batteries, most research efforts have focused on intelligent duty cycling and energy saving techniques at all layers of the protocol stack. Recent developments in energy harvesting technology from ambient sources promise to alleviate some of these concerns [1].

This paper explores the scenario where radio frequency (RF)-based technology is used to charge the sensors through dedicated *energy transmitters* (ETs). However, the high broadcast power of the ETs, emitting *energy waves* up to 3 Watts, introduces additional interference in data communication. Through detailed experimentation, this paper aims at quantifying the impact of selecting network parameters relevant to RF energy transfer and data communication on the coexistence of ETs and sensor nodes. In particular, we are interested in determining values of those parameters that enable fruitful coexistence, considering the challenges imposed by the low transmission power of the sensor nodes (e.g., the output power of 802.15.4 devices, which is typically as low as 0 dBm) and the high-power energy waves (possibly above 30 dBm), causing interference and significant packet loss.

Our experiments involve both the physical layer and the link layer by measuring the received signal strength, packet reception rate, and the amount of harvested power under carefully-designed scenarios with single and multiple ETs. Previous empirical studies in WSNs focused on complex, non-ideal behavior of low-power wireless links [2], [3], concurrent data transmissions [4], and the coexistence between WSNs and WiFi [5], [6], microwave ovens [7] and the smart grid [8]. To the best of our knowledge, this paper provides the first study on interference and coexistence issues in RF energy-powered WSNs. In so doing, we identify the boundary conditions that allow nodes equipped with RF energy harvesters to transfer data with high throughput and with limited interference from transmitting ETs.

The key contributions of our work include the following.

- We investigate the effect of data transmissions and energy transfer in the same frequency band, quantifying the impact of long-range interference of energy transmitters, and the energy charging range required to effectively recharge nodes.
- We show the interference between RF energy transmitters and wireless nodes when they occur simultaneously as a function of the separation of frequency of use. We also identify safe frequency separation for concurrent data and energy transmission.
- We demonstrate the destructive interference effect of multiple energy transmissions on the same frequency, and measure the impact of energy cancellation on the amount of harvested power.
- We show the viability and efficiency of multi-frequency band RF energy harvesting for RF energy circuits with a wide frequency response range.

The rest of this paper is organized as follows. In Sec-

tion II we describe our experimental setup. Section III presents results on determining viable ranges for coexistent WSNs and ETs. Results on concurrent data and energy transmissions are discussed in Section IV. Results concerning concurrent energy transmissions from multiple ETs are illustrated in Section V and VI. The paper is concluded in Section VII.

II. Experimental Setup

We selected a controlled environment with four plain walls and no other intermediate reflective objects to limit time-varying changes in the wireless channel due to multi-path fading and shadowing. We use a pair of Mica2 motes equipped with Chipcon CC1000 radios [9] operating at 915 MHz for the sensor nodes with a default RF (data) transmission power of 0 dBm. The receiver sensitivity is -98 dBm. Motes use a 38.4 Kbps data rate with Manchester encoding and a non-coherent FSK modulation scheme. For the RF frequency-tunable ET, we use an Agilent N5181 MXG RF signal generator [10] connected to an amplifier with a 50 Ω omnidirectional antenna in the 902–928 MHz band. Our setup also deploys commercially available P2110 RF energy harvesters from Powercast Co. [11], connected to the motes. The Agilent E5061B vector network analyzer is used to measure the strength of interfering signals caused by the ETs. The motes and ETs are placed on a flat table, 0.5 m from the floor. The sender and receiver nodes are placed one meter from each other, and they are equidistant from the ET. We use a total of 360 packet transmission epochs to estimate the packet reception rate (PRR) with a precision of 1.2% for each particular combination of energy transmission frequency and distance between the ET and the motes.

III. Ranges for Coexistent WSNs and ETs

In this section we determine ET ranges that affect mote charging and data communications. We are concerned about data communication among motes, as well as communications between motes and the ETs, for energy requests, control packet exchange and to relay traffic. More precisely, we are interested in determining: C_1: The *charging range* within which a mote can harvest RF energy and recharge its batteries. C_2: The *data communication* range within which a mote can communicate with the ET. However, motes in the circular area determined by $C_2 - C_1$ cannot be charged. C_3: The *interference range*. Motes in the circular area determined by $C_3 - C_2$ cannot be charged or communicate with the ET. Motes within the C_3 range experience interference from the ET energy transmission and therefore data communications among them is affected when the ET is charging the motes. These ranges are depicted in Fig. 1.

In the rest of this section we introduce the RF wireless charging model, and perform experiments to determine the maximum ranges for charging, communication and interference.
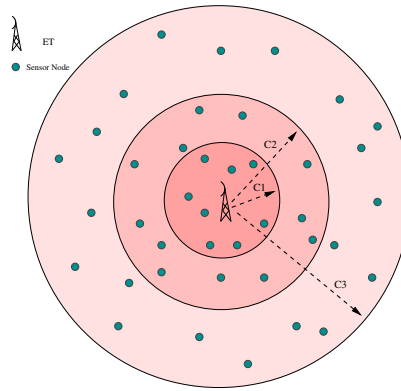

Fig. 1: The wireless charging (C_1), communication (C_2) and interference (C_3) ranges.

A. RF wireless charging model

According to Friis' free space model, the amount of RF power received by the energy harvesting circuit of the mote decreases with the square of the distance between the transmitter and the receiver. As a consequence, the available power and charging rate decreases for increasing distances between the ET and a mote. This means that after a certain distance, there would not be enough input power for the energy harvesting circuit to charge the node. Moreover, the incident RF radiation on the energy harvesting antenna is converted to a DC voltage using the RF energy harvester. The total RF-to-DC conversion efficiency of a node, which is defined as the ratio of output DC power to the incident RF power, depends on the design of the energy harvesting circuit and on the received RF power. The output voltage from the harvester (i.e., the available DC power after conversion) is then either stored in an energy storage component or delivered to the sensor node for immediate usage. Based on the Friis' free space model, the following formula provides a first-order estimate of the amount of power that may be harvested:

$$P_r = \eta G_{ET} G_r (\frac{\lambda}{4\pi D})^2 P_{ET}, \qquad (1)$$

where P_{ET} is the output power of the ET, η is the RF-to-DC conversion efficiency, G_{ET} is the antenna gain of the ET, and G_r is the antenna gain of the RF energy harvester. Also, D indicates the distance between the ET and the mote, and $\lambda = c/f_c$ is the wavelength of the radiated power, with c indicating the velocity of light and f_c the frequency chosen for energy transmission.

B. Charging range

We perform experiments to determine the maximum charging range and demonstrate the accuracy of Equation (1). We use the Powercast P2110 evaluation board [11]. The average wavelength of the energy signals transmitted at $f_c = 915$ MHz is 0.328 m, and the energy transmitter and RF energy harvesting circuit have antenna gains of 1 dBi and 6.1 dBi, respectively. The harvested energy is stored in a capacitor with capacitance rating $C = 100$
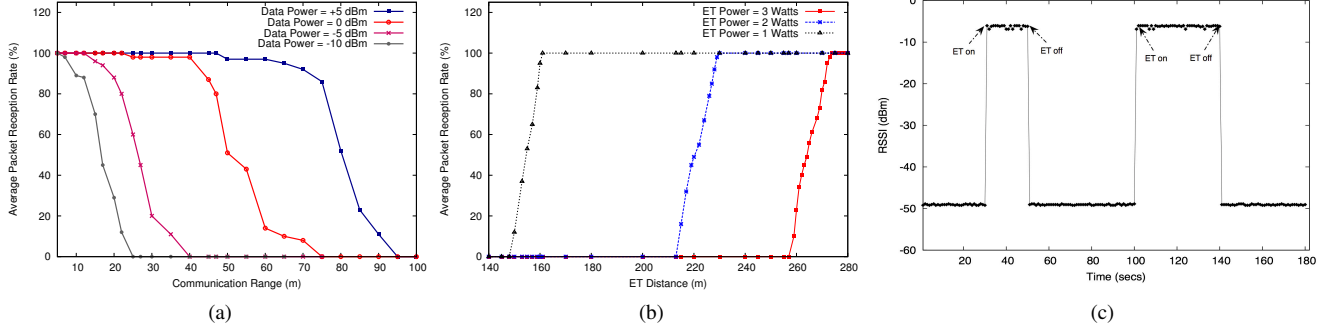
Fig. 3: (a) Communication ranges for different data transmit powers. (a) Energy transmission interference for different ET powers. (c) RSS for concurrent data and energy transfer at the same frequency.
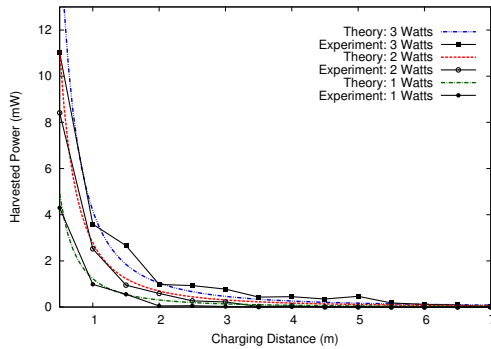

Fig. 2: Charging ranges: experiments vs. theory.

mF. We set the energy transmitter output power to 3, 2, and 1 Watts. The Federal Communications Commission (FCC) in the US limits the output power of radios using unlicensed frequency bands to 4 Watts effective isotropic radiated power (EIRP), and, accordingly, the ETs usually send power at maximum level of 3 Watts. We vary the distance between the antennas of the harvester and that of the ET from 0.5 to 7 m, in increments of 0.5 m. At each location, we measure the wireless charging duration ΔT starting from an initial voltage $V_1 = 1.8$ V, as minimum operating voltage of the Mica2, to $V_2 = 3.3$ V, as the maximum voltage of the capacitor, and calculate the harvested power using the relation: $C(V_2^2 - V_1^2)/2\Delta T$.

Fig. 2 shows curves for the experimental and theoretical results (Equation (1)) on the average harvested power as a function of the distance between the ET and the mote for three different transmit power settings. The theoretical and experimental curves are remarkably close. It can be observed that the measured harvested power significantly depends on the charging distance as well as on the ET transmission power. Furthermore, it is shown that when the mote is far away from the ET, the harvested RF power is negligible, and after a threshold the sensor node cannot effectively harvest any amount of useful energy. As depicted in Fig. 2, at the highest transmit power (3 Watts) the measured maximum charging range C_1 is about

5 m. The charging ranges for energy powers of 2 and 1 Watts are 3 and 1.5 m, respectively. The RF-to-DC conversion efficiency (η) in Equation (1), which depends on the received input RF power at a given location, is obtained from the Powercast P2110 harvester data-sheet [11].

C. Communication range

The data communication range between the mote and the ET and among sensor motes in an RF-powered WSN may be influenced by several factors such as the data transmission power, the sensitivity of the receiver node, the gain and efficiency of the antennas, and the transmission rate. To quantify the communication range, we assume the ET uses the same RF transceiver chip as the motes. We plot packet reception rate for different combinations of data transmission power and the separation distance between the sender and the receiver when the ETs are turned off. Specifically, we vary the straight line distance between two Mica2 motes and obtain PRR measurements at transmission power levels of 5, 0, -5, and -10 dBm, as shown in Fig. 3a. We observe that for each data transmit power, when the distance increases beyond a threshold, the packet reception rate decreases dramatically. We consider the threshold at which the percentage of received packets drops below 85% as an estimate of the communication range. Accordingly, from Fig. 3a we observe that the maximum communication ranges C_2 are approximately 75 m, 50 m, 20 m, and 12 m for data transmit powers of 5, 0, -5, and -10 dBm, respectively. It can be observed that the measured communication ranges are relatively longer than the charging ranges.

D. Interference range

We investigate the interference range C_3 of the ETs and how different energy transmission powers affect it. To this end, we use a pair of communicating Mica2 motes and vary the distance between the receiver mote and the ET under different output power levels. In particular, at each location, we measure the PRR over 360 packet transmission epochs for each of the three energy transmission values.

ET Power	Charging Range (C_1)	Interference Range (C_3)
1 Watts	1.5 m	160 m
2 Watts	3 m	230 m
3 Watts	5 m	275 m

Data Power	Communication Range (C_2)
+5 dBm	75m
0 dBm	50m
−5 dBm	20m
−10 dBm	12m

TABLE I: Summary of measured coexistence ranges in wireless-powered sensor network.

From Fig. 3b, we observe that for each transmit power there is a threshold distance at which the percentage of correctly received packets reaches zero. When the distance increases beyond that threshold, the percentage of received packets starts to increase gradually. This threshold is the interference range C_3. We observe that the interference ranges are significantly larger than both of the communication and the charging ranges obtained from Fig. 2 and 3a. We see in Fig. 3b that the maximum interference range is 160 m, 230 m, and 275 m when the ET transmits at 1, 2 and 3 Watts, respectively. Table I compares all the measured ranges for charging, communication, and interference.

IV. CONCURRENT DATA AND ENERGY TRANSMISSIONS

In this section, we investigate how high power energy transfer affects concurrent low power data transmissions among motes. We perform two different sets of experiments depending on whether energy and data transmissions happen at the same or at different frequencies.

A. Transmissions at the same frequency

We set the distance between the receiver mote and the ET to 5 m, the value of the maximum charging range. Packets are transmitted back to back from the sender to the receiver mote. The ET transfers power at 915 MHz, with an output power of 3 Watts. The ET is switched on at 30 s from the start of the experiment, turned off at 50 s, turned on again at 100 s and finally turned off at 140 s. The experiment terminated after 180 s. The level of interference in a channel is determined by measuring the received signal strength (RSS) values in the receiver, with the measured ambient noise having a standard deviation of less than 1 dBm.

Fig. 3c shows that without interference, the sender node has reliable communication with the destination. However, when the ET is turned on, the received power at the receiver mote increases noticeably from −50 dBm (data plus noise floor) to −6 dBm (joint data, noise, and interference). This leads to no packet reception during the transmission of energy signals.

B. Transmissions at different frequencies

The long interference ranges of ETs motivates us to investigate how PRR is affected by energy waves at frequencies different than those used for data communication.
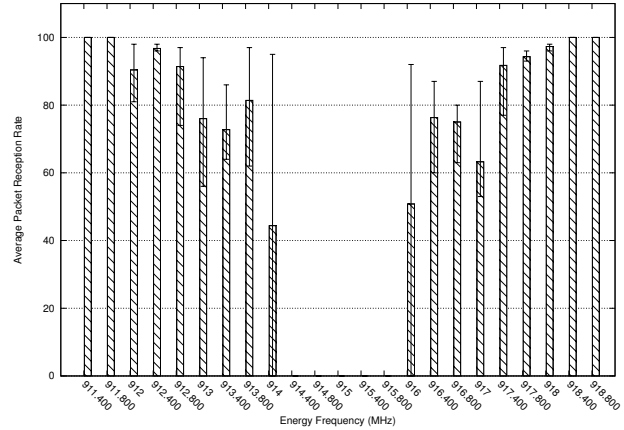

Fig. 4: The average PRR for varying energy transmission frequencies.

Interference may still occur because the transmission power of high radiative energy signals may leak into the data communication channel. This leakage power is a function of the separation between two channels used for energy and data transmission.

For this investigation we set the operating frequency for data communications to 915 MHz, and we vary the energy transfer frequency from 911 MHz to 919 MHz, while the power output of the ET is set to 3 Watts. For each frequency, we change the distance between the ET and the receiver mote from 1 m to 5 m (the maximum charging range), and measure the average PRR over all ranges. Note that these short ET ranges represent the worst case of interference, and as the ET distance increases, the packet reception rate improves. In Fig. 4 the bars indicate the average PRR over all ET ranges, and the error bars show the maximum and minimum PRRs among all distances as the frequency of energy transfer varies.

The results reveal the interference patterns between the ET and the mote when concurrent energy and data transmission happens at different frequencies, regardless of their distance. We find that the energy spectrum can be divided into three different areas: The one characterized by severe interference, the one by moderate packet reception, and the one with no packet loss. Table II summarizes these frequency areas. From Fig. 4, it can be observed that any energy transmission from 914.400 MHz to 915.800 MHz results in corruption of all data packets. In fact, the sensor data channel is still affected by the leakage power of energy signals transmitting on these frequencies, which results in 0% PRR. However, there are two spectral ranges, namely, from 913 MHz to 914 MHz and from 916 MHz to 917 MHz, where the average PRR is between 40% to 90%. This means that when the ET transfers energy over these frequency ranges, data transmissions will not always be successful, though at some frequencies high PRR is achieved. Fig. 4 shows that any energy transmission at frequencies less that 913 MHz or larger than 917 MHz
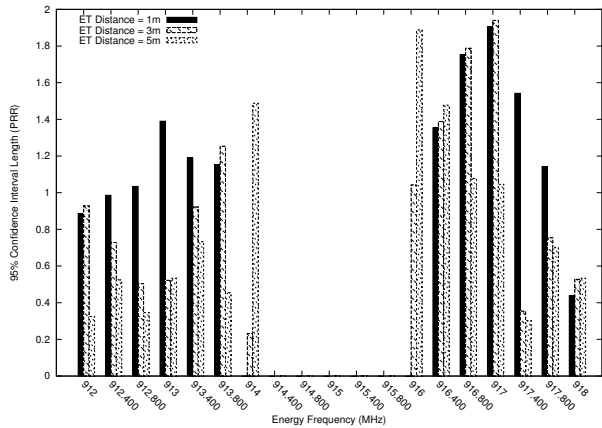
Fig. 5: The 95% confidence interval of PRR over different distances and frequencies.

Average PRR Range	Energy Frequency Range	$\Delta f(e,d)$
0%	914.400 − 915.800 MHz	less than 1 MHz
40% − 90%	913 − 914 MHz	1 to 2 MHz
	916 − 917 MHz	
90% − 100%	$f_e < 913$ MHz	2MHz
	$f_e > 917$ MHz	

TABLE II: Energy spectral ranges in concurrent energy and data transmission.

does not affect the PRR significantly. We observe that the average PRR in this case is always $\geq 90\%$.

Based on our experiments, we are able to determine a safe frequency separation distance $\Delta f(e,d)$ between energy and data signals such that if energy transmission and data transmission happen concurrently at frequencies that are separated more than $\Delta f(e,d)$, data transmission occurs without considerable interference.

In our testbed we find that the value of $\Delta f(e,d)$ is 2 MHz. Knowing this value can be useful for designing communication protocols for RF-powered sensor networks to guarantee concurrent data and energy transmissions over different frequencies without packet losses. Finally, Fig. 5 shows the 95% confidence interval of the average PRR for all selected distances between the ET and the receiving mote.

V. CONCURRENT ENERGY TRANSMISSIONS: SAME FREQUENCY

In this section we study the feasibility and the effects of energy transmissions from multiple ETs operating at the same frequency. We first investigate the constructive and destructive interference of concurrent energy transmissions and determine the energy cancellation range for concurrently transmitting ETs.

A sensor node can be charged either through a unilateral energy transfer of one ET, or through the coordinated transmission of multiple ETs. When a node requests energy from neighboring ETs, other nodes within the ET charging range also benefit from the energy transmission and can be recharged. In the case of multiple ETs, concurrent energy transmissions can only be beneficial if the arriving energy waves at the node are aligned in phase [12]. More specifically, the multiple energy waves can combine constructively or destructively according to their relative phases or path lengths between the energy transmitters and the receiver node, leading to variations in the amount of harvestable power. In constructive interference (in-phase), the received power of the resulting wave at the RF energy harvester is greater than that of either of the individual energy waves. In the case of destructive interference (out-phase), the net received power is less than that of the individual energy waves. Constructive and destructive interference depend on the relative distance from the ETs and the receiving nodes. Therefore, there will be areas where energy combines constructively and areas where energy waves cancel each other.

Fig. 6 depicts examples of constructive and destructive areas when two and three ETs transmit at the same frequency. These areas map out the way in which the phase difference between the energy waves varies in space. Here, the middle of the black circles represents crests of energy waves and the middle of the white circles represents the troughs. The energy waves interfere and cancel each other to some degree in the destructive areas (wedges of white) and strengthen each other within the constructive areas (wedges of dark). The patterns of constructive and destructive areas depend on the number and the separation of energy transmitters. As the number of ETs increases, it becomes quite involved to accurately estimate the power intensity distribution, and the pattern of the constructive and destructive areas.

Next, we perform a set of experiments to better understand and illustrate the effects of destructive and constructive interference. We consider two energy transmitters, ET1 and ET2, with the same configuration used for the charging range measurements in Section III-B. The ETs transfer energy at 915 MHz (i.e., $\lambda = 0.328$ m) each with an output power of 3 Watts. The ET and RF energy harvesting circuits have antenna gains of 1 dBi and 6.1 dBi, respectively, and the capacitor storage of the receiver node is $C = 100$ mF. We measure the total harvested power while varying the distances between energy transmitters and the receiver, which leads to the different phase separations of the arriving energy waves. In particular, we fix the path length between ET1 and the receiver mote at distances of 1, 2, and 3 meters, and at each location we vary the distance between ET2 and the antennas of the RF harvester from 0.5 to 6 meters. We repeat each experiment 10 times, and for each we record the wireless recharge duration and calculate the total harvested power (see Section III-B).

Fig. 7 compares our measurement results for different distances of ET1 and ET2. It can be observed that destructive interference from one ET strongly affects the energy transmitted by another ET, and at distances, all transmitted energy waves could be canceled totally. This results in
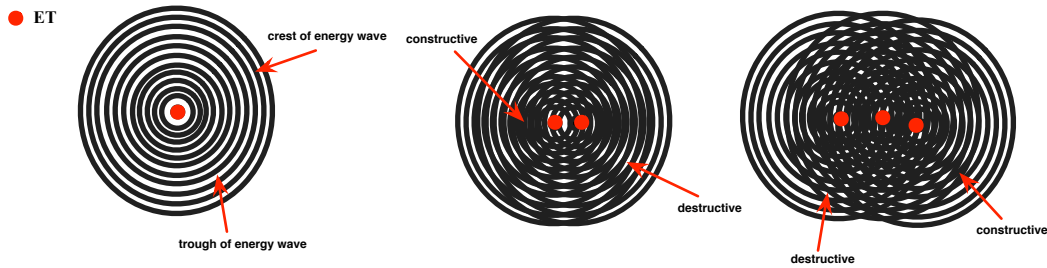
Fig. 6: Multiple energy transmitters at the same frequency cancel transferred energy in destructive areas and aggregate energy in constructive areas.
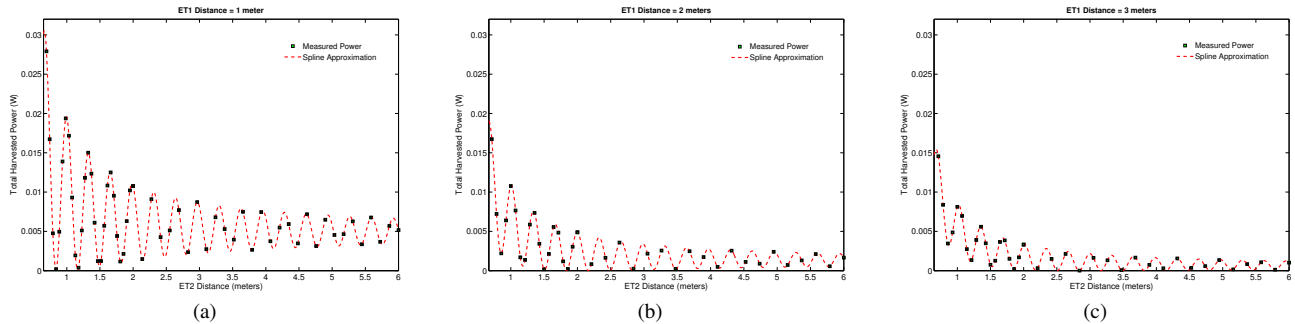

Fig. 7: Effect of destructive and constructive energy interference for two ETs. The distance between ET1 and the receiver is set to (a) 1 m, (b) 2 m, and (c) 3 m.

very low or no harvested power even when all ETs are transferring energy with high power. Also, this figure shows that there are distances in which the energy signals arrive constructively and the total measured harvested power in this case can be as much as four times the power of a single energy wave if the two energy transmitters have the same path length. Moreover, it is shown that the total measured harvested power oscillates between constructive and destructive values as the ET moves from one location to another.

From Fig. 7, we see that the interference from multiple energy transmissions depends on both the distance of the ETs from each other and the path length of each ET from the receiver mote. As the path length of the ET increases, the intensity of interference decreases, and after a threshold distance the destructive interference becomes negligible. On the other hand, comparing Fig. 7 (a), (b), and (c), we can see that the energy interference is more significant when the ETs are closer to the receiver. For example, the energy interference is higher when ET1 is 2 m away from the mote compared to when it is 3 m away. It is lower compared to when ET1 is 1 m away. Thus, interestingly, even though the ETs that are closer to the receiver provide higher levels of energy, they can result in higher levels of energy cancellation. This shows the importance of energy interference in the design of network protocols for RF-powered WSNs with multiple ETs.

The destructive and constructive interference of two incident energy waves are less pronounced when the power of one wave dominates the other, or when the power of both waves are very low. Let R_1 and R_2 denote the distances of

ET1 and ET2 from the receiver mote, respectively. Based on our experimental results, we define the energy cancellation range as the minimum path length difference of the two ETs ΔR_{min} with respect to the ET closer to the receiver and such that for all values of R_1 and R_2 for which $|R_2 - R_1| \geq \Delta R_{min}$ the joint energy interference has negligible effect on the amount of the total harvested power. The energy cancellation range could be useful in the design of routing protocols, for managing energy cancellation effects, and for channel assignment algorithms. The energy cancellation range is determined as follows. From Fig. 7, we see that when the first ET is located at distance 1 meter from the receiver, the effect of constructive and destructive energy interference in terms of fluctuations in the harvested power would be significant till ET2 is 2 m from the receiver. The energy interference decreases as the distance between ETs and the receiver increases, and the interference becomes negligible when ET2 is 5 m away. Accordingly, the energy cancellation range when ET1 is 1 m away from the receiver is found to be 4 meters. Similarly, the energy cancellation range when ET1 is to 2 and 3 meters away is be found to be 0 m, when ET2 is 2 m away, and 1.5 m when ET2 is 1.5 m away, respectively.

VI. Concurrent Energy Transmissions: Multi-Frequency

In this section, we show the feasibility and efficiency of RF energy harvesting at multiple frequencies (*multi-band RF harvesting*).

Fig. 8a and 8b show the harvesting efficiency of the P2110 and P1110 energy harvesters [11] over the full ISM
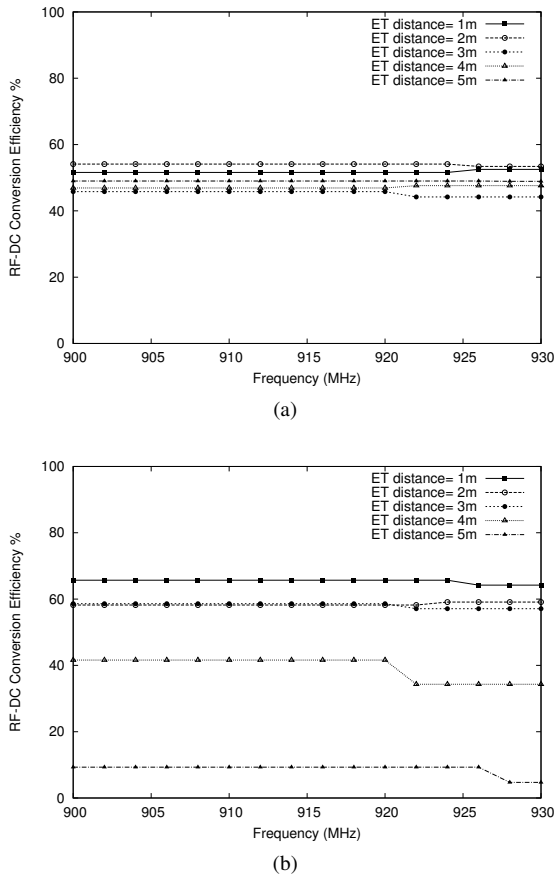
(a)

(b)

Fig. 8: RF harvesting efficiency between the RF harvester and the ET for Powercast P2110 (a) and P1110 (b) harvesting boards.

frequency range for 902 MHz to 928 MHz, for various ET-to-harvester distances. These results are obtained from the powercast RF harvester data-sheets as well as the powercast wireless charging calculator [11] that contains the RF-to-DC conversion efficiency at different frequencies and input powers. We can see that the efficiency of RF energy harvesting depends on the input power, which is a function of the distance between the ET and the RF harvester. Moreover, both pictures in Fig. 8 show that the design of the harvesting circuit has a significant impact on the efficiency of harvesting. Specifically, the P2110 powerharvester outperforms the P1110 harvesting board over long charging distances, while the P1110 harvesting board has better performance over short charging distances. Most important, at each distance the RF energy harvesting circuit provides almost the same performance and efficiency over a range of frequencies. As the bandwidth of the energy signal is relatively small (i.e., 99% of the occupied bandwidth is approximately 63 kHz [12]), our results demonstrate that if the RF harvester is optimized for a frequency range transferring energy at different frequencies will not decrease the amount of harvested power when using multiple ETs, independent of the distance between

the energy transmitters and the receivers. Consequently, the RF harvester can simultaneously and effectively harvest RF power over a range of different frequencies within the bandwidth of its harvesting circuit.

VII. CONCLUSIONS

We have presented an experimental investigation of concurrent energy and data transmissions in RF-powered WSNs. Our experiments have quantified the wireless charging, communication, and interference ranges for coexistent WSNs and wireless energy transmitters. We have shown the severe effect of high power energy waves on data communication and the energy cancellation of concurrent energy transmissions. We have demonstrated that frequency separation and multi-band RF harvesting are promising for enabling coexistence and improving general network performance and energy harvesting throughput.

REFERENCES

[1] S. Basagni, M. Y. Naderi, C. Petrioli, and D. Spenza, "Wireless sensor networks with energy harvesting," in *Mobile Ad Hoc Networking: Cutting Edge Directions*, S. Basagni, M. Conti, S. Giordano, and I. Stojmenovic, Eds. Hoboken, NJ: John Wiley & Sons, Inc., March 5 2013, ch. 20, pp. 703–736.

[2] K. Srinivasan, P. Dutta, A. Tavakoli, and P. Levis, "An empirical study of low-power wireless," *ACM Trans. on Sensor Networks*, vol. 6, no. 2, pp. 16:1–16:49, March 2010.

[3] J. Zhao and R. Govindan, "Understanding packet delivery performance in dense wireless sensor networks," in *Proceedings of ACM SenSys 2003*, 2003, pp. 1–13.

[4] D. Son, B. Krishnamachari, and J. Heidemann, "Experimental study of concurrent transmission in wireless sensor networks," in *Proceedings of ACM SenSys 2006*, 2006, pp. 237–250.

[5] D. Yang, Y. Xu, and M. Gidlund, "Wireless coexistence between IEEE 802.11- and IEEE 802.15.4-based networks: A survey," *Int. Journal of Distributed Sensor Networks*, vol. 2011, pp. Article ID 912 152, 17 pages, 2011.

[6] L. Angrisani, M. Bertocco, D. Fortin, and A. Sona, "Experimental study of coexistence issues between IEEE 802.11b and IEEE 802.15.4 wireless networks," *IEEE Trans. on Instrumentation and Measurement*, vol. 57, no. 8, pp. 1514–1523, 2008.

[7] K. R. Chowdhury and I. F. Akyildiz, "Interferer classification, channel selection and transmission adaptation for wireless sensor networks," in *Proceedings of IEEE ICC 2009*, 2009, pp. 1–5.

[8] V. Gungor, B. Lu, and G. Hancke, "Opportunities and challenges of wireless sensor networks in smart grid," *IEEE Trans. on Industrial Electronics*, vol. 57, no. 10, pp. 3557–3564, 2010.

[9] "CC1000 radio datasheet," Chipcon, 2014. [Online]. Available: http://www.ti.com/lit/ds/symlink/cc1000.pdf

[10] "N5181A MXG RF Analog Signal Generator," Agilent, 2014. [Online]. Available: http://cp.literature.agilent.com/litweb/pdf/5989-5311EN.pdf

[11] Powercast, http://www.powercastco.com, 2014.

[12] M. Naderi, P. Nintanavongsa, and K. Chowdhury, "RF-MAC: A medium access control protocol for re-chargeable sensor networks powered by wireless energy harvesting," *IEEE Transactions on Wireless Communications*, vol. 13, no. 7, pp. 3926–3937, July 2014.